

Article

Au Functionalized SnS₂ Nanosheets Based Chemiresistive NO₂ Sensors

Ding Gu ^{1,2}, Wei Liu ¹, Jing Wang ², Jun Yu ², Jianwei Zhang ^{2,*}, Baoyu Huang ^{1,*}, Marina N. Rumyantseva ³  and Xiaogan Li ¹

- ¹ School of Microelectronics, Dalian University of Technology, Dalian 116024, China; guding815@mail.dlut.edu.cn (D.G.); liuwei6@mail.dlut.edu.cn (W.L.); lixg@dlut.edu.cn (X.L.)
- ² Faculty of Electrical and Electronic Engineering, Dalian University of Technology, Dalian 116024, China; wangjing@dlut.edu.cn (J.W.); junyu@dlut.edu.cn (J.Y.)
- ³ Laboratory of Chemistry and Physics of Semiconductor and Sensor Materials, Chemistry Department, Moscow State University, Leninskie Gory 1-3, 199991 Moscow, Russia; roum@inorg.chem.msu.ru
- * Correspondence: jwzhang@dlut.edu.cn (J.Z.); huangby@dlut.edu.cn (B.H.)

Abstract: Layered Au/SnS₂ nanosheet based chemiresistive-type sensors were successfully prepared by using an in situ chemical reduction method followed by the hydrothermal treatment. SEM and XRD were used to study the microscopic morphology and crystal lattice structure of the synthesis of Au/SnS₂ nanomaterials. TEM and XPS characterization were further carried out to verify the formation of the Schottky barrier between SnS₂ nanosheets and Au nanoparticles. The as-fabricated Au/SnS₂ nanosheet based sensor demonstrated excellent sensing properties to low-concentrations of NO₂, and the response of the sensor to 4 ppm NO₂ at 120 °C was approximately 3.94, which was 65% higher than that of the pristine SnS₂ (2.39)-based sensor. Moreover, compared to that (220 s/520 s) of the pristine SnS₂-based sensor, the response/recovery time of the Au/SnS₂-based one was significantly improved, reducing to 42 s/127 s, respectively. The sensor presents a favorable long-term stability with a deviation in the response of less than 4% for 40 days, and a brilliant selectivity to several possible interferents such as NH₃, acetone, toluene, benzene, methanol, ethanol, and formaldehyde. The Schottky barrier that formed at the interface between the SnS₂ nanosheets and Au nanoparticles modulated the conducting channel of the nanocomposites. The “catalysis effect” and “spillover effect” of noble metals jointly improved the sensitivity of the sensor and effectively decreased the response/recovery time.

Keywords: SnS₂ nanosheets; noble metals; NO₂ detection; gas sensor; charge transfer



Citation: Gu, D.; Liu, W.; Wang, J.; Yu, J.; Zhang, J.; Huang, B.; Rumyantseva, M.N.; Li, X. Au Functionalized SnS₂ Nanosheets Based Chemiresistive NO₂ Sensors. *Chemosensors* **2022**, *10*, 165. <https://doi.org/10.3390/chemosensors10050165>

Academic Editor: Manuel Alexandre

Received: 5 April 2022

Accepted: 27 April 2022

Published: 28 April 2022

Publisher's Note: MDPI stays neutral with regard to jurisdictional claims in published maps and institutional affiliations.



Copyright: © 2022 by the authors. Licensee MDPI, Basel, Switzerland. This article is an open access article distributed under the terms and conditions of the Creative Commons Attribution (CC BY) license (<https://creativecommons.org/licenses/by/4.0/>).

1. Introduction

As a precursor of photochemical smog and acid rain, nitrogen dioxide gas is a typical poisonous and corrosive atmospheric pollution. It is produced from the combustion of fossil fuel and automobile exhaust [1]. Excessive nitrogen dioxide gas generated in the air would lead to a decrease in atmospheric visibility, acidification of soil and water, and corrosion of buildings [2,3]. It also poses a threat to the health of human beings. Long-term exposure to ppm-level NO₂ would be particularly dangerous to human health, especially to the respiratory system, and may cause lung malfunction [4]. Furthermore, the detection of nitrogen oxides (NO_x) in the human respiration system is currently applied to the diagnosis of human diseases, which is a non-invasive diagnostic method [5]. For instance, ppb-level NO_x in human exhaled gases is an important biomarker for diagnosing inflammatory airway disease [6,7]. In addition, NO_x can be used as biological indicators for lung diseases [8–10]. Therefore, it is of great significance to develop a simple and reliable NO₂ gas sensor.

Metal sulfides have triggered the interests of researchers in detecting NO₂ gas at low temperatures or even room temperature due to its unique crystal structure and hysic-

chemical properties [11–14]. Compared with traditional metal oxides, most metal sulfides are stacked by a two-dimensional single-layer sheet structure, which make it a narrower band gap, a larger specific surface area, and more active sites. These advantages are beneficial to the adsorption and desorption of gas molecules on the surface of the nanomaterials. Among these metal sulfide materials, tin disulfide (SnS_2) is a typical layered two-dimension structure nanomaterial, which has been studied in the field of gas sensing detection [15–17]. Ou et al., synthesized a novel gas sensor based on two-dimensional SnS_2 flakes, which has a good sensitivity to NO_2 [18]. Liu et al., investigated the sensing behavior of nanosheet-assembled SnS_2 nanoflowers prepared by a simple hydrothermal method [19]. Gu et al., explored the gas sensing characteristics of a SnS_2 nanosheet under visible light illustrated at room temperature [20]. However, it is still a challenge to improve the response and recovery speeds of SnS_2 -based sensors.

The modification and doping of noble metal nanoparticles on gas sensing materials have been proven to be one of the most effective methods to prolong the lifetime of semiconductor carriers and improve the adsorption capacity of gas molecules on sensitive materials, which could be attributed to the “electronic sensitization” and “spillover effect” of noble metals [21–23]. Noble metal/semiconductor heterostructure is an ideal mode for improving the gas performance of semiconductor materials. For instance, Au nanoparticles exhibit excellent catalytic effect at sizes smaller than 10 nm, and it is also the least active noble metal toward atoms and molecules [24,25]. Functionalization of Au nanoparticles with high catalytic activity can not only promote the adsorption of gas molecules on the surface of the material, but can also accelerate the chemical reaction between the adsorbed oxygen and the target gas.

Hence, Au nanoparticles with excellent catalytic performance were selected to decorate the SnS_2 material in order to enhance the response value and improve the response/recovery speeds of the SnS_2 -based sensor to NO_2 at the low temperature region by the synergistic effect of “electron sensitization” and “chemical sensitization”. The Au functionalized SnS_2 nanosheets with different Au contents was synthesized by a simple in situ chemical reduction method and the gas sensing performance was also systematically investigated. The research results show that the sensor-based on the Au/ SnS_2 -0.5 sample greatly enhanced the sensing performance to NO_2 of the SnS_2 -based sensor at low temperature region (129 °C), which exhibited a fast response/recovery speed, excellent signal reproducibility, a good long-term stability, and anti-interference ability. The sensing mechanism of the sensor is discussed in detail.

2. Experimental

2.1. Preparation of SnS_2 Nanosheet

The SnS_2 nanosheets were fabricated through the hydrothermal method. A total of 233 mg $\text{SnCl}_2 \cdot 2\text{H}_2\text{O}$, 499 mg $\text{Na}_2\text{S}_2\text{O}_3 \cdot 5\text{H}_2\text{O}$, and 160 mg sulfur powder were added into a 50 mL Teflon-lined autoclave, which had been pre-filled with deionized water to 80% of its capacity. The Teflon-lined autoclave was maintained in a muffle furnace at 200 °C for 12 h, and then naturally cooled to room temperature. The filtered yellow precipitates were washed several times with deionized water, carbon disulfide, and ethanol to remove the residuals of sulfur and organic solvents.

2.2. Decoration of Au Nanoparticles on the Surface of SnS_2 Nanosheets

Figure 1 illustrates the scheme for decorating the Au nanoparticles on the surface of SnS_2 nanosheets. Au functionalized SnS_2 nanosheets were performed by in situ chemical reduction of the HAuCl_4 by using $\text{C}_6\text{H}_5\text{Na}_3\text{O}_7$ as the reducing agent. A total of 100 mg of as-synthesized SnS_2 nanosheets were dispersed into 30 mL of deionized water and ultrasonically sonicated for 30 min to form a uniform dispersion. Subsequently, 0.05 mL of HAuCl_4 (0.01 M) was added into the above solution. After 10 min, 0.15 mL of $\text{C}_6\text{H}_{14}\text{N}_2\text{O}_2$ solution (0.01 M) was added into the mixture and stirred with a magnetic stirrer at room temperature for 30 min. After stirring for 30 min, a certain amount of Au ions were

doped on the SnS₂ nanosheets, and then 0.1 mL of 0.1 M trisodium citrate solution was added and stirred for 30 min, so that the Au ions doped on the SnS₂ nanosheets could be chemically reduced to Au nanoparticles. The resultant product was washed several times with deionized water and absolute ethyl alcohol to remove the impurities. The washed precipitate was placed in a drying oven and dried at 60 °C for 12 h, thus obtaining the composite material of Au/SnS₂ nanosheets, which was defined as Au/SnS₂-0.5. For a comparison, the corresponding amounts of chloroauric acid, L-lysine, and trisodium citrate solution were added according to the proportion to prepare the Au/SnS₂-0.1, Au/SnS₂-0.3, Au/SnS₂-1, and Au/SnS₂-1.5 composites.

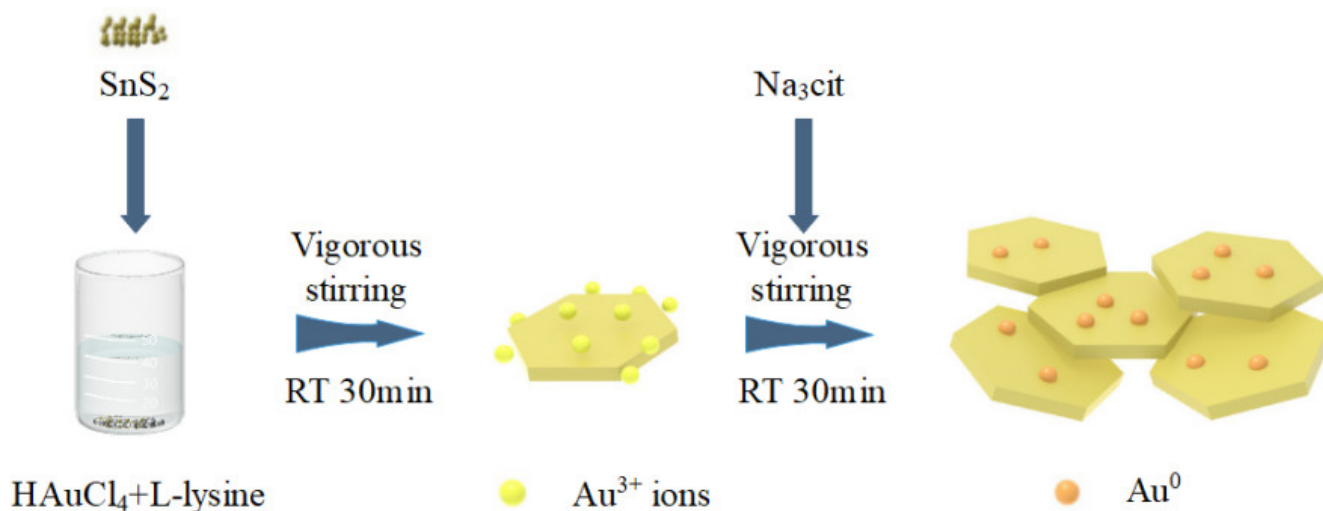


Figure 1. Schematic view of modifying Au nanoparticles on SnS₂ nanosheets.

2.3. Preparation of Sensors

Figure 2 shows the structural diagram of the Au interdigital electrode with heating layer function, which was used as the substrate of the gas-sensing material to transmit the chemiresistive sensing signal in this work. The front side of the interdigital electrode is the gold electrode, which is made by printing gold paste on the surface of the alumina ceramic substrate through the screen printing process and then sintering at high temperature (850 °C). The width of each golden interdigital finger and the distance between adjacent interdigitated fingers were both 200 μm, and the gas sensing material was deposited on the surface of the gold electrode by the dip-coating method. The backside of the interdigital electrode had the heating function, which consisted of a RuO₂ resistive layer and Ag/Pb pads. The RuO₂ resistance layer will reach the different working temperatures by applying corresponding DC voltages between the ends of the Ag/Pb pads. A sample of 10 mg of powdered Au/SnS₂ nanocomposite and a small amount of deionized water were added to a mortar and ground for 5 min to form a uniform slurry. The resulting paste material was then dripped onto the forked finger electrode, which was then dried in an oven at 60 °C for 12 h to obtain a sensor for sensitive performance testing.

2.4. Material Characterization

The crystal structure of the as-prepared Au/SnS₂ was recorded using X-ray diffraction (XRD: XRD-6000, Shimadzu Corp, Tokyo, Japan) at a scanning rate of 0.26°/s from 10° to 75°. The scanning electron microscope (SEM: S-3000 N, Hitachi, Japan) and the transmission electron microscope (TEM: Tecnai G220, Philips, The Netherlands) were used to record the microscopic morphology and crystal lattice sizes of the synthesis of Au/SnS₂ nanomaterials. The information of the elemental and chemical states were recorded by a Thermo ESCALAB 250Xi X-ray photoelectron spectrometer with an Al Kα source ($h\nu = 1486.6$ eV). The beam spot diameter of the monochrome Al source was 500 μm and the power was 150 W.

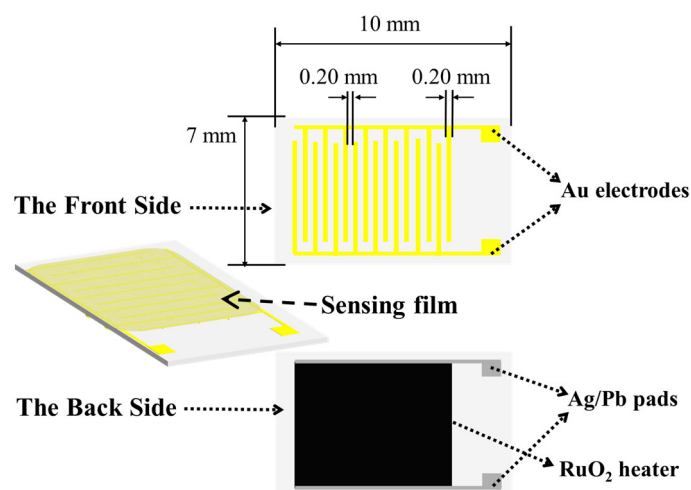


Figure 2. Structure diagram of the Au interdigital electrodes.

2.5. Gas Sensing Measurements

The gas sensing performances of the sensors were measured by using fully automatic computer controlled gas distribution and data acquisition systems under a dynamic gas flow region. Various parameters such as the bias voltage, the testing time, and the concentration of the target gases were controlled by the computer. The Agilent 34465A computer-controlled multimeter recorded the electrical resistance of the sensors. The responses (S) of the sensors were defined as the relative change in the resistance of the sensors in the background and those in the tested gas (Equations (1) and (2)):

$$S = \frac{R_g}{R_a} \quad (\text{for NO}_2) \quad (1)$$

$$S = \frac{R_a}{R_g} \quad (\text{for other reducing gases}) \quad (2)$$

where R_a and R_g are the stable resistances of sensor in the air and in the tested gases. The response or recovery times of the sensors were defined as the time taken for the sensor to achieve 90% change in the full magnitude change of the gas response.

3. Results and Discussion

3.1. Microstructure Characterization of As-Synthesized Au/SnS₂ Nanosheets

Figure 3 shows the XRD spectra of the Au/SnS₂ nanocomposites with different proportions. It can be clearly observed from Figure 3a in the XRD spectrogram that there were obvious diffraction peaks at 15.03 and 28.20° in the spectrograms of Au/SnS₂-0.1, Au/SnS₂-0.3, Au/SnS₂-0.5, Au/SnS₂-1, and Au/SnS₂-1.5, respectively. The (001), (100), (101), (110), and (111) crystal planes of SnS₂ corresponding to the 2T structure were consistent with JCPDF#23-0677. However, the existence of elemental Au was not detected in the composite materials with 0.1%, 0.3%, 0.5%, and 1%, which may be due to the much lower content of Au doped in the composite materials than the lowest detection limit of XRD equipment. However, when the doping ratio of Au nanoparticles in the composite reached 1.5%, a weak diffraction peak of the Au element appeared at 38.18° (corresponding card: JCPDF#04-0784).

It can be observed from the enlarged view of the local diffraction peak on the (001) crystal plane in Figure 3b that the diffraction peaks of the Au/SnS₂ composite materials had a slight shift with an angle of 0.17 to 0.22°. It indicates that during the doping process, some Au atoms may enter the SnS₂ lattice and be doped into the SnS₂ lattice or sulfur vacancy. At the same time, with the increase in Au doping content, the diffraction peak intensity of the Au/SnS₂ composites became weak, which may be related to the agglomeration of

SnS₂ nanosheets caused by the use of a higher concentration of trisodium citrate in the process of reduction of a high proportion of Au, which can also be further confirmed from the later SEM results of the composites. In addition, no other diffraction peaks for any impurities were found in the XRD spectra, which also proved that the prepared Au/SnS₂ nanomaterials had high purity.

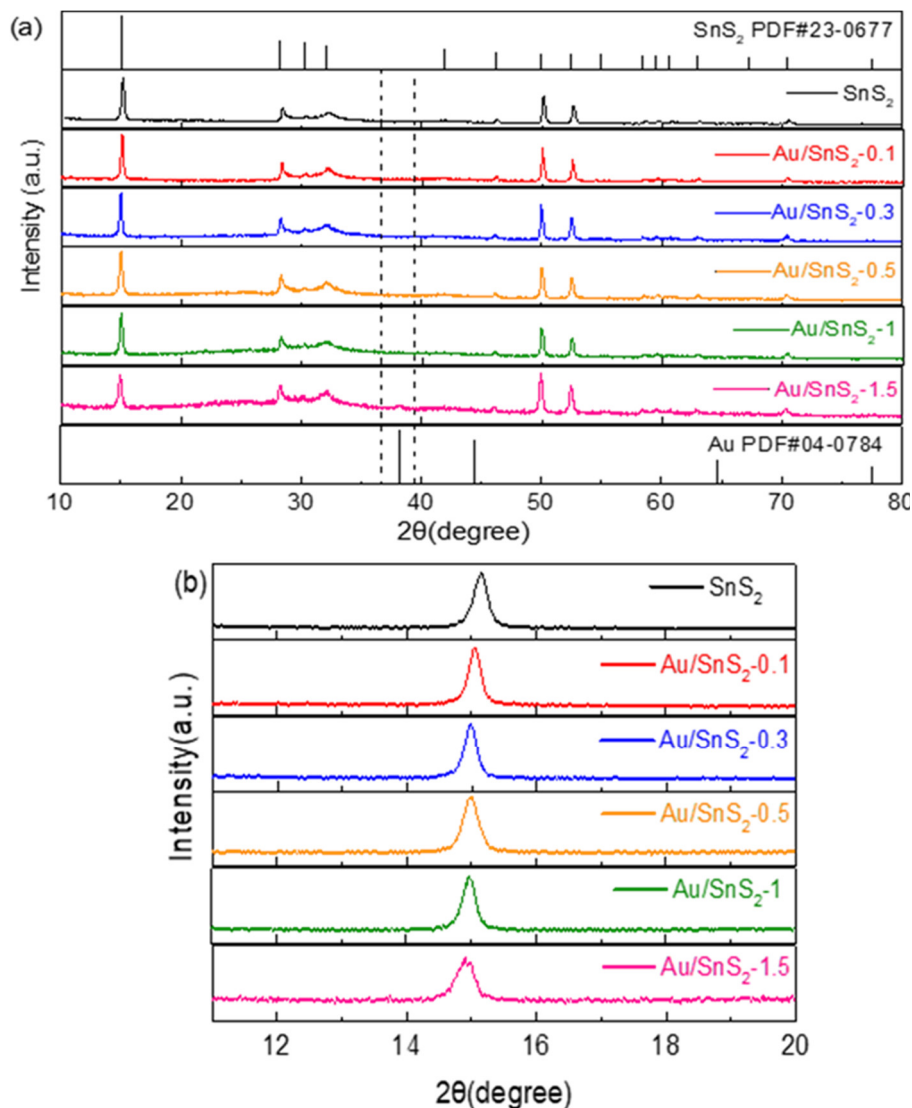


Figure 3. (a) XRD patterns of the prepared samples and (b) partial enlarged view of the XRD.

Figure 4 shows the SEM images of the SnS₂, Au/SnS₂-0.5, and Au/SnS₂-1.5 nanocomposites. It can be observed that the pristine SnS₂ had a layered-nanosheet structure with particle sizes ranging from 50 nm to 500 nm, as shown in Figure 4a. In the Au/SnS₂ nanocomposite, due to the reduced Au nanoparticle size being smaller than the detection limit of the SEM equipment, no obvious Au nanoparticles were observed, and the specific shape of Au nanoparticles could not be clearly observed. However, with the increase in Au doping concentration, the surface of the SnS₂ nanosheets in the composites began to agglomerate, and it was obviously observed that there were agglomerated SnS₂ nanosheets in Au/SnS₂-1.5, as shown in Figure 4b,c. This phenomenon was perhaps due to the reduction in the high doping amount of Au, and the content of the reducing agent trisodium citrate also increased, which resulted in the agglomeration between small and medium-sized SnS₂ nanosheets during the reduction process. Figure 4d shows the EDS characterization results of the Au/SnS₂-0.5 nanocomposites. It can be observed that the Au/SnS₂-0.5 nanocompos-

ites contained Au, S, and Sn elements with the atomic ratio of Au:S:Sn of 66.99:33.36:0.15, and the mass percentage of Au was approximately 0.47 wt%, which was slightly lower than the nominal value (0.5 wt%). This result indicates that the Au element was indeed introduced into the Au/SnS₂ nanocomposites in this experiment and the existing form of the Au element will be studied by further characterization.

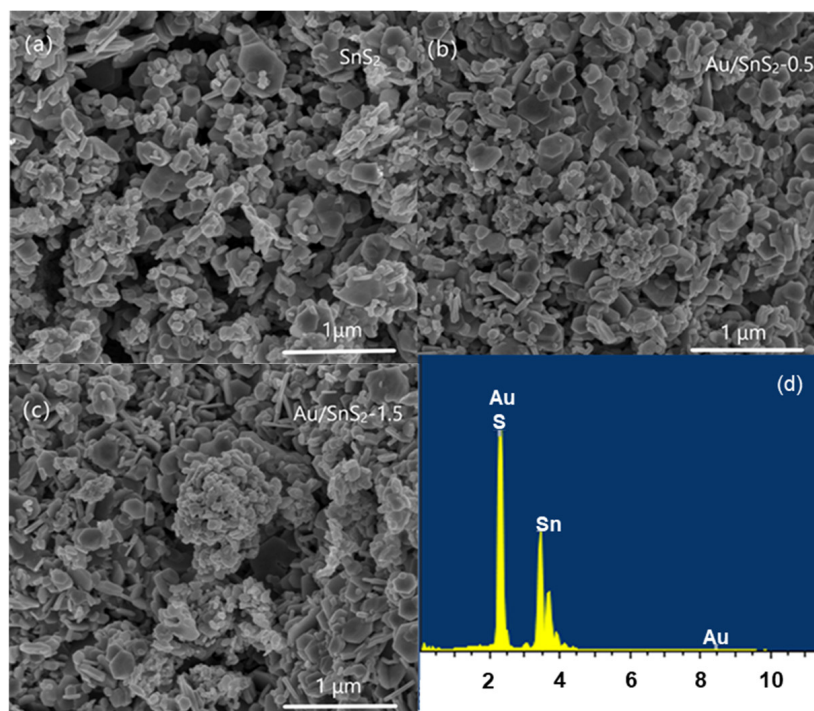


Figure 4. SEM images of (a) SnS₂, (b) Au/SnS₂-0.5, (c) Au/SnS₂-1.5, and (d) EDS elemental estimation of the Au/SnS₂-0.5 sample.

To further investigate the crystal phase structure of the Au/SnS₂ nanocomposites, TEM images of the SnS₂ nanosheets and Au/SnS₂-0.5 nanocomposites are shown in Figure 5. Figure 5a,b reveals that the pristine SnS₂ nanosheets had a hexagonal flake morphology, and the distance between two adjacent groups of lattice stripes was 0.290 nm, which corresponded to the (002) crystal plane of SnS₂, and no lattice stripes of other substances appeared. Figure 5c shows the morphology of the Au/SnS₂-0.5 nanocomposites had no obvious change, and it was still a layered structure. It notes that rough nanoparticles appeared on the flat surface of the SnS₂ nanosheets in Figure 5d, with an average size of about 5 nm, and the spacing between two adjacent groups of stripes was 0.236 nm, which is consistent with the (111) crystal plane spacing of Au. This demonstrates that the small-sized nanoparticles on the surface of SnS₂ were Au nanoparticles, which further confirms that the Au nanoparticles had been successfully decorated on the SnS₂ nanosheets by the chemical reduction method.

X-ray photoelectron spectroscopy (XPS) was performed to characterize and analyze the chemical components and elemental states on the surface of pristine SnS₂ nanosheets and Au/SnS₂ nanocomposites. Figure 6 shows the XPS spectra of the SnS₂ nanosheets and Au/SnS₂-0.5 composite nanomaterials. The C1s peak at 284 eV belonged to foreign hydrocarbons from the XPS instrument itself, which was used as the calibration peak. Figure 6a shows the full survey spectra of the pristine SnS₂ and Au/SnS₂-0.5 samples, which all contained characteristic peaks of the Sn, S, and O elements. There was a weak peak at around 86 eV, which was assigned to the Au⁰ in the Au/SnS₂-0.5 nanocomposites. Figure 6b–e displays the high-resolution spectra and fitting curves of O 1s, Sn 3d, S 2p, and Au 4f of the SnS₂ nanosheets and Au/SnS₂-0.5 composites in a small energy range.

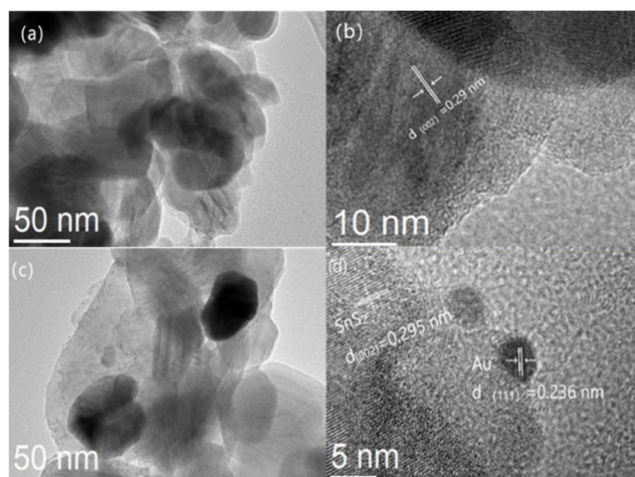


Figure 5. (a) TEM image of SnS₂, (b) HRTEM image of SnS₂, (c) TEM image of Au/SnS₂-0.5, and (d) HRTEM image of Au/SnS₂-0.5.

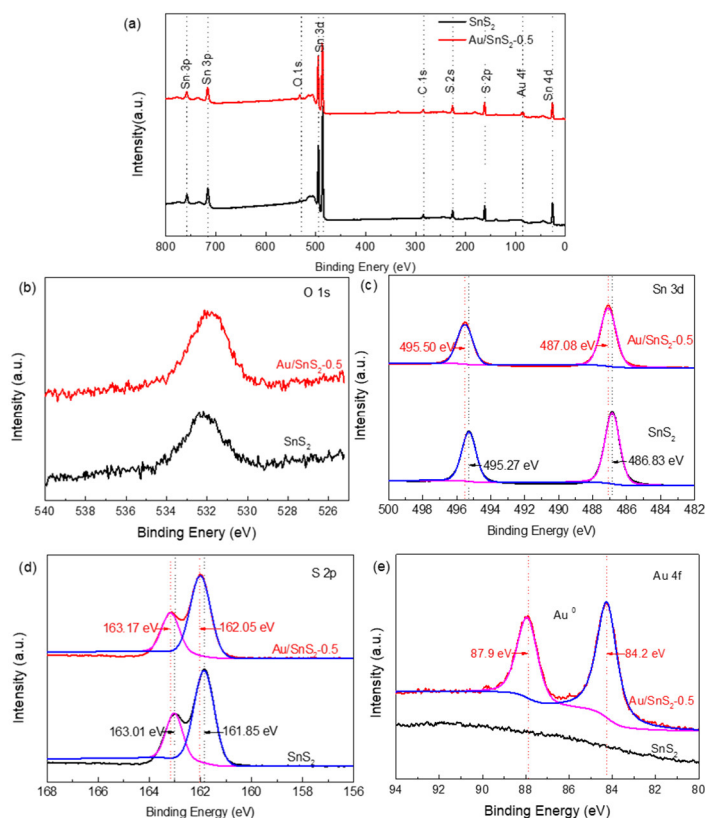


Figure 6. XPS spectra of SnS₂ and Au/SnS₂-0.5: (a) full survey spectra of samples, (b) O 1s region, (c) Sn 3d region, (d) S 2p region, and (e) Au 4f region.

As shown in Figure 6b, the peak that appeared at 532.2 eV in the O 1s spectrum of the pristine SnS₂ nanosheet corresponded to the chemisorbed oxygen (O_{2(ads)}⁻ or O_(ads)⁻) on the surface of the sample [26,27]. No lattice oxygen (O²⁻) could be observed, indicating that SnS₂ did not contain the impurity phase of metal oxides such as SnO₂. Compared with the pristine SnS₂, the O 1s peak of the Au/SnS₂-0.5 composite had a higher peak intensity of chemisorbed oxygen, indicating that the decoration of noble metals promoted the adsorption of chemisorbed oxygen molecules by the sample. The chemisorbed oxygen on the surface of the Au/SnS₂-0.5 sample could participate in subsequent redox reactions

with NO₂ molecules. Thus, it is beneficial to improve the gas-sensing performance of the Au/SnS₂-0.5-based sensor.

The refined spectra of the Sn 3d of pristine SnS₂ and Au/SnS₂ composites was further analyzed as shown in Figure 6c. It was found that both samples contained Sn 3d peaks, and the energy difference between Sn 3d_{5/2} and Sn 3d_{3/2} peaks was approximately 8.4 eV, which indicates that the chemical state of SnS₂ did not change during the Au reduction process, and Sn ions were still at the highest oxidation state of +4 [28]. Compared to the pristine SnS₂, the fitting peak of Sn 3d in the Au/SnS₂-0.5 composite shifted to higher binding energy, and the binding energy increased to approximately 0.2 eV. This shift indicates that Au has a certain influence on the electronic state of SnS₂ shell, and the electrons transfer from the conduction band of SnS₂ to Au.

Figure 6d shows the S 2p spectrums of two samples. The two peaks centered at 161.85 eV and 163.01 eV corresponded to S 2p_{3/2} and S 2p_{1/2}, respectively [29,30]. It was also found that the fitting peak of S 2p in the Au/SnS₂-0.5 sample shifted to a higher energy level. This was due to the work function of Au (5.10 eV) being higher than that of SnS₂, which causes the electrons in the outer shell of SnS₂ to be attracted to the core of Au. This kind of charge transfer regulates the electron concentration on the surface of Au/SnS₂-0.5, resulting in electron-hole separation. The spectra of Au elements in the two samples are shown in Figure 6e. There was no Au characteristic peak in the SnS₂ material, but there were obvious Au double peaks in the Au/SnS₂-0.5 sample, which were located at 87.9 eV and 84.2 eV, respectively, corresponding to Au 4f_{7/2} and Au 4f_{5/2} [31,32]. This indicates that Au in the Au/SnS₂-0.5 composite was successfully reduced and SnS₂ was decorated by the metal Au.

3.2. Gas-Sensing Property of Au/SnS₂ Nanosheets

For the gas sensor, the working temperature is one of the important parameters that affect the performance of the sensor. Figure 7 reveals the response of SnS₂, Au/SnS₂-0.1, Au/SnS₂-0.3, Au/SnS₂-0.5, Au/SnS₂-1, and Au/SnS₂-1.5-based sensors to 4 ppm NO₂ at the operating temperatures from 100 °C to 180 °C. The response of pristine SnS₂-based sensor first increased and then decreased with the increase in temperature, and the response value reached the maximum at the working temperature of 120 °C, which was approximately 2.39. The response of Au-doped SnS₂-based sensors had the same changing trend with the working temperatures. At low content Au, the optimal working temperature of the Au/SnS₂-0.1, Au/SnS₂-0.3, and Au/SnS₂-0.5-based sensors was at 120 °C, which indicates that Au decoration does not reduce the working temperature of the SnS₂ nanomaterial, but improved the NO₂ sensitivity of the sensor. With the further increase in Au content, the optimal working temperature of Au/SnS₂-1 and Au/SnS₂-1.5-based sensors was 140 °C, which was higher than that of the pristine SnS₂-based one. This is perhaps due to the increase in the proportion of sodium citrate added in reducing the high concentration Au, which causes the small-sized SnS₂ nanosheets to agglomerate during the reduction of noble metals, and the materials were denser. This is consistent with the results of the SEM, as shown in Figure 4.

The response of the composite material was higher than that of pristine SnS₂ with the increase in Au concentration when less than 1 wt%. The response values of the Au/SnS₂-0.1, Au/SnS₂-0.3, Au/SnS₂-0.5, and Au/SnS₂-1-based sensors at 120 °C were 2.54, 3.12, 3.94, and 2.94, respectively. When the doping ratio was greater than 1%, the response of the Au/SnS₂-1.5-based sensors instead became lower than that of the pristine SnS₂-based one. According to literature [33,34], when the size of Au nanoparticles is less than 5 nm, it shows excellent catalytic activities. The Au nanoparticles became agglomerates to form large-sized particles when Au content was high as shown in SEM results. The agglomerated Au nanoparticles usually have poor catalytic performance, which might induce the poor sensing properties of Au/SnS₂-1.5-based sensor.

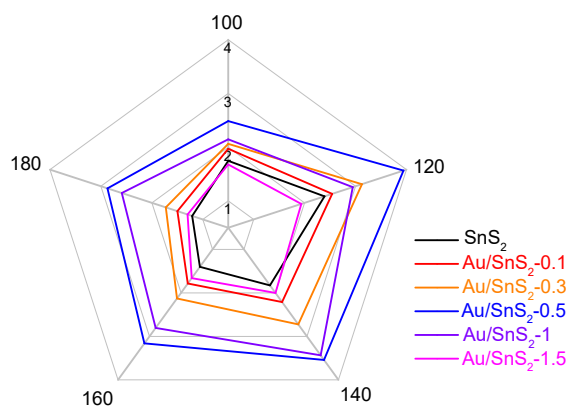


Figure 7. The response of as-fabricated sensors to 4 ppm NO_2 in the temperature range of 100 °C to 180 °C.

Figure 8 shows the response and resistance curves of the Au/SnS₂ composites and SnS₂ materials with different Au amounts to 4 ppm NO_2 at their respective optimal working temperatures. Figure 8a shows that when the composite was doped with Au at a low concentration, the resistance of the composite increased with the increase in the doping amount of Au particles. However, further increasing the Au content to more than 1%, the resistance of the composite material decreased. As the Au content increased, the number of Au nanoparticles gathered on the surface of the SnS₂ increased, the particle size became larger, and agglomerates between Au nanoparticles occurred, which improved the conductivity of the composite material and reduced the resistance. When the sensor was exposed to 4 ppm NO_2 , the resistance of the sensor increased rapidly. Then, the resistance of the sensor achieved a stable plateau. The resistance of the sensor decreased and gradually returned to the initial resistance after NO_2 was terminated. Both SnS₂ and the Au/SnS₂ composites showed typical n-type semiconductor characteristics.

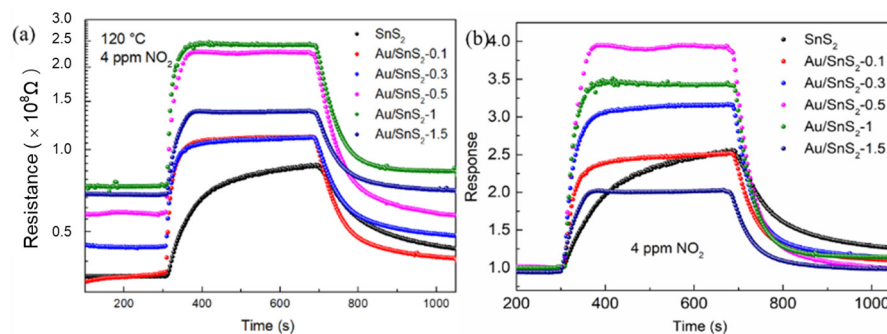


Figure 8. (a) The resistance and (b) the response curves of SnS₂, Au/SnS₂-0.1, Au/SnS₂-0.3, Au/SnS₂-0.5, Au/SnS₂-1, and Au/SnS₂-1.5-based sensors to 4 ppm NO_2 at 120 °C.

Figure 8b shows the response curves of the Au/SnS₂ composites with different Au content and the pristine SnS₂-based sensors to 4 ppm NO_2 at the optimal working temperatures. When the Au concentration increased from 0.1 wt% to 0.5 wt%, the sensing performance of the composite material was better than that of pristine SnS₂, and the response value to 4 ppm NO_2 increased with the increase in Au content. When the Au concentration was 0.5 wt%, the sensing characteristics of the composite material were the best. When the Au content was higher than 1 wt%, the response value of the composite gradually decreased. At the same time, the response and recovery time of the composite materials to 4 ppm NO_2 at the optimal temperature were significantly shorter than that of pristine SnS₂. The experimental results showed that 0.5 wt% was the optimum doping concentration of Au particles for the SnS₂ nanosheet materials.

Response/recovery time is an important performance parameter of a gas sensor. Figure 9 is a comparison diagram of the response curves of the Au/SnS₂-0.5 composite

material and pristine SnS₂ nanosheet material to 4 ppm NO₂. It can be clearly observed from the figure that the response value (3.94) of the Au/SnS₂-0.5 composite to 4 ppm NO₂ was higher than that of pristine SnS₂ nanosheet (2.39). The decoration of Au nanoparticles not only significantly improved the response value of SnS₂, but also greatly shortened the response/recovery time of SnS₂ nanomaterials to NO₂. Compared with pristine SnS₂, the response/recovery time of Au/SnS₂-0.5 was 42 s/127 s, which was reduced 5.0/4.1 times shorter than that of the pristine SnS₂ nanosheet material (220 s/520 s). This demonstrates that Au-decoration could enhance the sensing performance of SnS₂ and effectively promote the adsorption and desorption process of NO₂ molecules on the surface of SnS₂ nanomaterials.

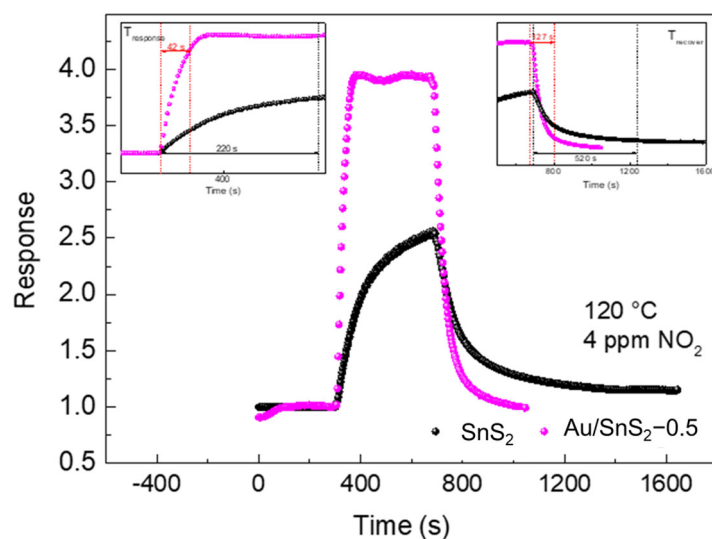


Figure 9. The response of SnS₂ and Au/SnS₂-0.5-based sensors to 4 ppm NO₂ at 120 °C, and the inset images are the response/recover time of the samples.

The response curve of the Au/SnS₂-0.5-based sensor from 0.25 ppm to 8 ppm NO₂ at 120 °C is shown in Figure 10a. The sensor showed a quick response to NO₂. The resistance of the sensor gradually returned to the initial when the NO₂ was terminated. The Au/SnS₂ composite sensor had excellent response and recovery characteristics in the range of 0.25 ppm to 8 ppm NO₂. Meanwhile, with the increase in the NO₂ concentration, the response of the Au/SnS₂-0.5 composite material increased. The response value of the Au/SnS₂-0.5 composite material under different concentrations of NO₂ was fitted, as shown in Figure 10b. The correlation curve between the response value of the Au/SnS₂ composite material and NO₂ was approximately linear. Furthermore, the theoretical detection limit (LOD) of the Au/SnS₂-0.5-based sensor can be estimated by Equations (3) and (4), according to a signal/noise not less than 3 [35,36].

$$\text{LOD} = 3 \times \text{RMS}_{\text{noise}} / \text{slope} \quad (3)$$

$$\text{RMS}_{\text{noise}} = \sqrt{\sum_{i=1}^n (R_i - \bar{R})^2 / N} \quad (4)$$

where R_i is the response measured experimentally before NO₂ exposure; \bar{R} is the average response value; and N is the number of the data point. The theoretical LOD was thus calculated to be approximately 50 ppb using the slope of the fitted linearity of the response versus NO₂ concentration and the root-mean-square (RMS_{noise}) deviation at the baseline. This shows that the decorated Au nanoparticles can improve the sensing performance of the SnS₂-based sensor for the detection of NO₂.

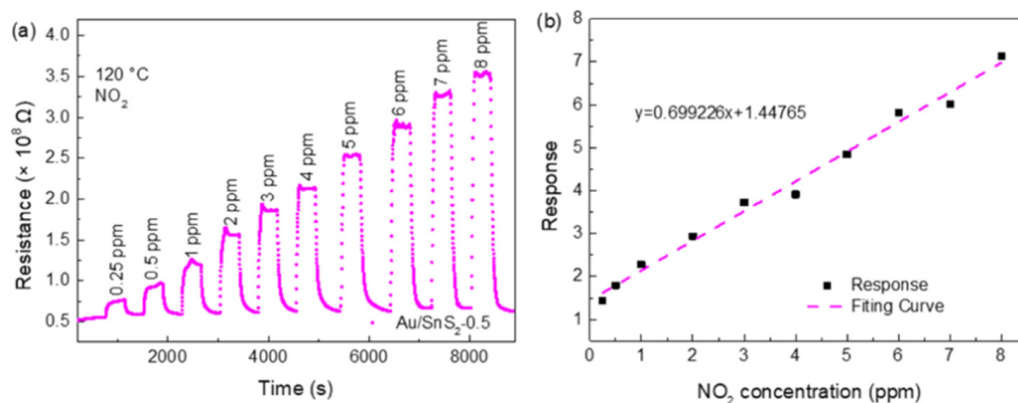


Figure 10. (a) The resistance curve of the Au/SnS₂-0.5-based sensor to 0.25 ppm–8 ppm NO₂ at 120 °C. (b) The fitting curve of the response of the sensor with NO₂ concentrations.

Figure 11 shows the response of the Au/SnS₂-0.5 composite to different interfering gases of 5 ppm at the optimal working temperature (120 °C), in which the interfering gases include NH₃, acetone, toluene, benzene, methanol, ethanol, and formaldehyde. The experimental results showed that the Au/SnS₂-0.5 composite exhibited the highest response to NO₂ gas. Although the SnS₂-based sensor had a certain response to NH₃, the response was far less than that of NO₂. This is perhaps due to the fact that SnS₂ has a tendency to adsorb N with a unique lone-pair polarity in the gas molecules, which makes NO₂ gas molecules react with the material surface at even lower temperatures, while other interfering gases need higher energy to undergo adsorption and desorption with the material surface. Therefore, the SnS₂ showed extremely low sensitivity to other interfering gases at a lower working temperature, showing excellent selectivity to NO₂. This excellent selectivity remained unchanged with the decoration of Au nanoparticles.

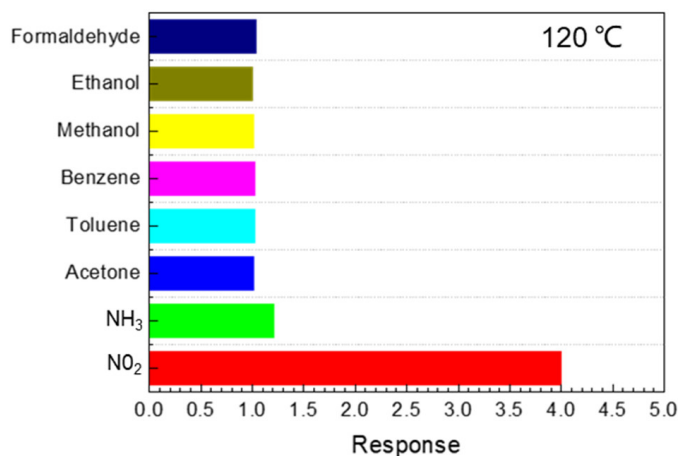


Figure 11. The selectivity of the Au/SnS₂-0.5-based sensor to 4 ppm NO₂ and several possible interfering gas species.

Figure 12a reveals the signal reproducibility of the Au/SnS₂-0.5-based sensor to 4 ppm NO₂ at 120 °C. It shows that the resistance of the Au/SnS₂-0.5-based sensor had no obvious change after five consecutive measurements, and the average response value was approximately 4.0, which indicates that the Au/SnS₂-0.5 composite had superior signal repeatability. Figure 12b shows the long-term stability of the Au/SnS₂-0.5-based sensor for 4 ppm NO₂ at 120 °C. After 40 days of continuous gas sensing measurements, the response value of the sensor to NO₂ was stable and basically remained unchanged. The deviation of the response of the sensor was calculated to be less than 4%, which indicates that the SnS₂ nanosheets decorated with Au nanoparticles have brilliant stability. Table 1 shows the performance comparison between the SnS₂ sensor in this work and the previously reported

SnS₂-based NO₂ sensor. It can be seen that the Au/SnS₂ sensor in this work showed relatively high response and fast response and recovery rate at the low temperature region. In addition, it should be mentioned that this Au/SnS₂ material had a problem of high resistance. In future research work, further attempts will be made to reduce the resistance of Au/SnS₂ materials by compositing Au/SnS₂ materials with some sensitive materials with ultra-high room temperature conductivity (including carbon nanotubes, graphene, and WTe₂, etc.) or using laser irradiation to meet the practical application requirements, which has been proven to be feasible in previous work [20].

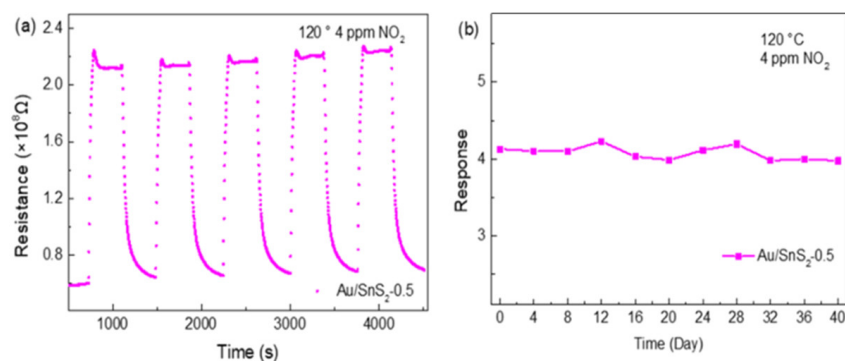


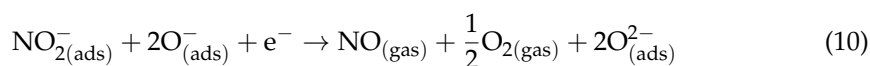
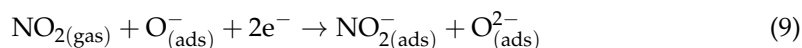
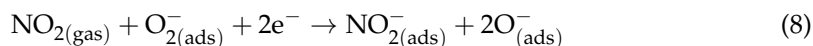
Figure 12. (a) The repeatability of the Au/SnS₂-0.5-based sensor to 4 ppm NO₂ at 120 °C. (b) The long-term stability of the sensor.

Table 1. A comparison of the NO₂ sensing performance of SnS₂-based sensors.

Sensing Material	Target Gas	Concentration (ppm)	Temperature (°C)	Response	Response/Recovery Time	Ref.
SnS ₂ nanoflowers	NO ₂	0.1	120	5.7	850 s/1050 s	[19]
SnS ₂ -nanosheets	NO ₂	10	250	2.49	4 s/40 s	[12]
SnS ₂ -nanosheets	NO ₂	10	120	4.7	120 s/170 s	[18]
SnO ₂ /SnS ₂	NO ₂	8	80	5.3	159 s/297 s	[26]
Au/SnS ₂ -0.5	NO ₂	4	120	3.94	42 s/127 s	This work

3.3. Gas-Sensing Mechanism

As shown in Figure 13, due to the different work functions between the SnS₂ semiconductor and Au nanoparticles, the work function of SnS₂ was smaller than that of Au, and charge transfer occurred across the Au/SnS₂ interface [37,38]. The charge was transferred from the conduction band of SnS₂ to Au nanoparticles through the interface when Au nanoparticles were successfully deposited onto the SnS₂ nanosheets until the Fermi level of SnS₂ and Au reached final equilibrium. The Schottky contact was thus formed at the interface between the SnS₂ and Au nanoparticles. Compared to the pristine SnS₂, the Schottky contact formed at the interface between SnS₂ and Au in the composite material narrowed the electronic conducting channel of the Au/SnS₂, and the potential barrier difference of the Au/SnS₂ changed more after NO₂ adsorption and the redox reaction occurred on the surface of the sensing materials according to the below reactions:



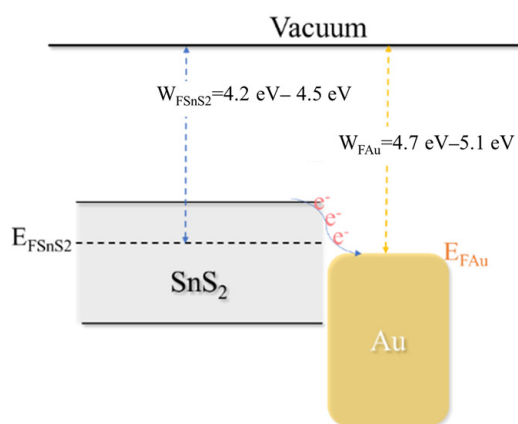


Figure 13. Schematic diagram of the charge transfer between the SnS₂ nanosheet and Au nanoparticles.

This led to the larger change in the resistance of the Au/SnS₂-based sensor.

The small-sized Au nanoparticles aggregated together when more Au above 1 wt% was decorated in the SnS₂ matrix, resulting in the decrease in active sites between the SnS₂ nanosheets and Au nanoparticles. The reduction in the catalytic efficiency of noble metals led to the deterioration of the gas sensing performance of the sensor. In addition, the inherent characteristics of Au nanoparticles allows it to play a dual role in the gas sensing process of the composite material. During the sensor's transducing process, Au nanoparticles can not only serve as electron donors to increase the number of carriers in the reaction between the composite material surface and the gas molecules, but they can also serve as electron acceptors to effectively separate the carriers generated in the semiconductor, prolonging the life of electron-hole and shortening the response/recovery time of the sensor.

The noble metal Au not only has the function of “electron sensitization”, but also has the function of “chemical catalysis” [39,40]. Compared to the pristine SnS₂ nanosheets, Au nanoparticles decorated on the surface of the Au/SnS₂ composites were also equivalent to the active sites of the gas sensing reaction. Given the “spillover effect” of noble metals, gas molecules adsorbed on the surface of the Au nanoparticles will further “spillover” to the surface of the SnS₂ nanosheets, which leads to an increase in the number of active sites on the surface of Au/SnS₂ composite materials [41,42]. Furthermore, Au nanoparticles can effectively promote the ionization of oxygen molecules and reduce the activation energy of the gas molecules, which makes realization of the dynamic equilibrium of the transducing reaction at a lower working temperature. As a result, the response/recovery time of the Au/SnS₂ composites decrease and the performance of the sensor is improved.

4. Conclusions

The Au/SnS₂ nanocomposites were successfully prepared by the hydrothermal and in situ reduction methods. The enhancement in the sensing performance of two dimensional structured SnS₂ nanosheets by the decoration of Au was explored. It was found that the particle morphology and content of Au had a significant influence on the gas sensing performance of the Au/SnS₂ composites. The Au/SnS₂-0.5 sample with the optimum gold content could significantly improve the sensitivity, response, and recovery rate of the SnS₂-based material to a low concentration NO₂ gas at a low temperature region. At 120 °C, the response of the Au/SnS₂-0.5 nanocomposite to 4 ppm NO₂ gas was 3.94, which was significantly higher than that of the original SnS₂ material (2.39). Moreover, the modification of Au nanoparticles could also significantly optimize the response and recovery characteristics of the SnS₂-based sensor. The response/recovery time of the Au/SnS₂-0.5-based sensor to 4 ppm NO₂ gas at 120 °C was shortened to 42 s/127 s. The sensor also presented a favorable long-term stability with a deviation in the response of less than 4% for 40 days, and a brilliant selectivity to several possible interferents such as NH₃, acetone, toluene, benzene, methanol, ethanol, and formaldehyde. The enhanced sensing

performance could be attributed to the synergistic effects from the “electronic sensitization” and “chemical sensitization” furnished by Au nanoparticles introduced in the SnS₂ matrix, which makes it a promising candidate material for preparing high-performance NO₂ gas sensors.

Author Contributions: Conceptualization, investigation, data curation, formal analysis, software, visualization, original draft preparation, D.G.; Investigation, data curation, visualization, original draft preparation, W.L.; Investigation, data curation, J.W.; Methodology, conceptualization, formal analysis, J.Y.; Resources, writing—review & editing, J.Z.; Supervision, conceptualization, writing—review & editing, B.H.; Resources, software, M.N.R.; Resources, funding acquisition, X.L. All authors have read and agreed to the published version of the manuscript.

Funding: The authors are thankful to the National Natural Science Foundation of China (Nos. 61971085, 62111530055, 61874018), the National Key R&D Program of China (No. 2021YFB3201302), the Russian Foundation for Basic Research (No. 21-53-53018) and the Fundamental Research Funds for the Central Universities of China (No: DUT19RC(3)054).

Institutional Review Board Statement: Not applicable.

Informed Consent Statement: Not applicable.

Data Availability Statement: Not applicable.

Conflicts of Interest: The authors declare no conflict of interest.

References

1. Saboor, F.H.; Ueda, T.; Kamada, K.; Hyodo, T.; Mortazavi, Y.; Khodadadi, A.A.; Shimizu, Y. Enhanced NO₂ gas sensing performance of bare and Pd-loaded SnO₂ thick film sensors under UV-light irradiation at room temperature. *Sens. Actuators B Chem.* **2016**, *223*, 429–439. [[CrossRef](#)]
2. Dai, Z.; Lee, C.S.; Tian, Y.; Kim, I.D.; Lee, J.H. Highly reversible switching from P- to N-type NO₂ sensing in a monolayer Fe₂O₃ inverse opal film and the associated P-N transition phase diagram. *J. Mater. Chem. A* **2015**, *3*, 3372–3381. [[CrossRef](#)]
3. Huang, Y.; Jiao, W.; Chu, Z.; Ding, G.; Yan, M.; Zhong, X.; Wang, R. Ultrasensitive room temperature ppb-level NO₂ gas sensors based on SnS₂/rGO nanohybrids with P-N transition and optoelectronic visible light enhancement performance. *J. Mater. Chem. C* **2019**, *7*, 8616–8625. [[CrossRef](#)]
4. Li, K.; Luo, Y.; Liu, B.; Gao, L.; Duan, G. High-performance NO₂-gas sensing of ultrasmall ZnFe₂O₄ nanoparticles based on surface charge transfer. *J. Mater. Chem. A* **2019**, *7*, 5539–5551. [[CrossRef](#)]
5. Liu, W.; Gu, D.; Li, X. Detection of Ppb-level NO₂ using mesoporous ZnSe/SnO₂ core-shell microspheres based chemical sensors. *Sens. Actuators B Chem.* **2020**, *320*, 128365. [[CrossRef](#)]
6. Kim, J.S.; Yoon, J.W.; Hong, Y.J.; Kang, Y.C.; Abdel-Hady, F.; Wazzan, A.A.; Lee, J.H. Highly sensitive and selective detection of ppb-level NO₂ using multi-shelled WO₃ yolk-shell spheres. *Sens. Actuators B Chem.* **2016**, *229*, 561–569. [[CrossRef](#)]
7. Moon, H.G.; Jung, Y.; Han, S.D.; Shim, Y.S.; Shin, B.; Lee, T.; Kim, J.S.; Lee, S.; Jun, S.C.; Park, H.H.; et al. Chemiresistive Electronic Nose toward Detection of Biomarkers in Exhaled Breath. *ACS Appl. Mater. Interfaces* **2016**, *8*, 20969–20976. [[CrossRef](#)]
8. Zhao, T.; Fu, X.; Cui, X.; Lian, G.; Liu, Y.; Song, S.; Wang, Q.; Wang, K.; Cui, D. An in-situ surface modification route for realizing the synergetic effect in P₃HT-SnO₂ composite sensor and strikingly improving its sensing performance. *Sens. Actuators B Chem.* **2017**, *241*, 1210–1217. [[CrossRef](#)]
9. Koo, W.T.; Choi, S.J.; Kim, N.H.; Jang, J.S.; Kim, I.D. Catalyst-decorated hollow WO₃ nanotubes using layer-by-layer self-assembly on polymeric nanofiber templates and their application in exhaled breath sensor. *Sens. Actuators B Chem.* **2016**, *223*, 301–310. [[CrossRef](#)]
10. Lee, S.W.; Lee, W.; Hong, Y.; Lee, G.; Yoon, D.S. Recent advances in carbon material-based NO₂ gas sensors. *Sens. Actuators B Chem.* **2018**, *255*, 1788–1804. [[CrossRef](#)]
11. Liu, L.; Ikram, M.; Ma, L.; Zhang, X.; Lv, H.; Ullah, M.; Khan, M.; Yu, H.; Shi, K. Edge-exposed MoS₂ nanospheres assembled with SnS₂ nanosheet to boost NO₂ gas sensing at room temperature. *J. Hazard. Mater.* **2020**, *393*, 122325. [[CrossRef](#)] [[PubMed](#)]
12. Kim, Y.H.; Phan, D.T.; Ahn, S.; Nam, K.H.; Park, C.M.; Jeon, K.J. Two-dimensional SnS₂ materials as high-performance NO₂ sensors with fast response and high sensitivity. *Sens. Actuators B Chem.* **2018**, *255*, 616–621. [[CrossRef](#)]
13. Hermawan, A.; Septiani, N.L.W.; Taufik, A.; Taufik, A.; Yulianto, B.; Yin, S. Advanced Strategies to Improve Performances of Molybdenum-Based Gas Sensors. *Nano-Micro Lett.* **2021**, *13*, 1–46. [[CrossRef](#)] [[PubMed](#)]
14. Xu, T.; Liu, Y.; Pei, Y.; Chen, Y.; Jiang, Z.; Shi, Z.; Xu, J.; Wu, D.; Tian, Y.; Li, X. The ultra-high NO₂ response of ultra-thin WS₂ nanosheets synthesized by hydrothermal and calcination processes. *Sens. Actuators B Chem.* **2018**, *259*, 789–796. [[CrossRef](#)]
15. Cheng, M.; Wu, Z.; Liu, G.; Zhao, L.; Gao, Y.; Zhang, B.; Liu, F.; Yan, X.; Liang, X.; Sun, P.; et al. Highly sensitive sensors based on quasi-2D rGO/SnS₂ hybrid for rapid detection of NO₂ gas. *Sens. Actuators B Chem.* **2019**, *291*, 216–225. [[CrossRef](#)]

16. Shafiei, M.; Bradford, J.; Khan, H.; Piloto, C.; Wlodarski, W.; Li, Y.; Motta, N. Low-operating temperature NO₂ gas sensors based on hybrid two-dimensional SnS₂-reduced graphene oxide. *Appl. Surf. Sci.* **2018**, *462*, 330–336. [[CrossRef](#)]
17. Huang, Y.; Jiao, W.; Chu, Z.; Wang, S.; Chen, L.; Nie, X.; Wang, R.; He, X. High Sensitivity, Humidity-Independent, Flexible NO₂ and NH₃ Gas Sensors Based on SnS₂ Hybrid Functional Graphene Ink. *ACS Appl. Mater. Interfaces* **2020**, *12*, 997–1004. [[CrossRef](#)]
18. Ou, J.Z.; Ge, W.; Carey, B.; Daeneke, T.; Rotbart, A.; Shan, W.; Wang, Y.; Fu, Z.; Chrimes, A.F.; Wlodarski, W.; et al. Physisorption-Based Charge Transfer in Two-Dimensional SnS₂ for Selective and Reversible NO₂ Gas Sensing. *ACS Nano* **2015**, *9*, 10313–10323. [[CrossRef](#)]
19. Liu, D.; Tang, Z.; Zhang, Z. Nanoplates-assembled SnS₂ nanoflowers for ultrasensitive ppb-level NO₂ detection. *Sens. Actuators B Chem.* **2018**, *273*, 473–479. [[CrossRef](#)]
20. Gu, D.; Wang, X.; Liu, W.; Li, X.; Lin, S.; Wang, J.; Romyantseva, M.N.; Gaskov, A.M.; Akbar, S.A. Visible-light activated room temperature NO₂ sensing of SnS₂ nanosheets based chemiresistive sensors. *Sens. Actuators B Chem.* **2020**, *305*, 127455. [[CrossRef](#)]
21. Kondalkar, V.V.; Duy, L.T.; Seo, H.; Lee, K. Nanohybrids of Pt-Functionalized Al₂O₃/ZnO Core-Shell Nanorods for High-Performance MEMS-Based Acetylene Gas Sensor. *ACS Appl. Mater. Interfaces* **2019**, *11*, 25891–25900. [[CrossRef](#)] [[PubMed](#)]
22. Sankar, G.R.; Navaneethan, M.; Patil, V.L.; Ponnusamy, S.; Muthamizhchelvan, C.; Kawasaki, S.; Patil, P.S.; Hayakawa, Y. Sensitivity enhancement of ammonia gas sensor based on Ag/ZnO flower and nanoellipsoids at low temperature. *Sens. Actuators B Chem.* **2018**, *255*, 672–683.
23. Li, F.; Guo, S.; Shen, J.; Shen, L.; Sun, D.; Wang, B.; Chen, Y.; Ruan, S. Xylene gas sensor based on Au-loaded WO₃·H₂O nanocubes with enhanced sensing performance. *Sens. Actuators B Chem.* **2017**, *238*, 364–373. [[CrossRef](#)]
24. Walker, J.M.; Akbar, S.A.; Morris, P.A. Synergistic effects in gas sensing semiconducting oxide nano-heterostructures: A review. *Sens. Actuators B Chem.* **2019**, *286*, 624–640. [[CrossRef](#)]
25. Zhang, D.; Yang, Z.; Li, P.; Pang, M.; Xue, Q. Flexible self-powered high-performance ammonia sensor based on Au-decorated MoSe₂ nanoflowers driven by single layer MoS₂-flake piezoelectric nanogenerator. *Nano Energy* **2019**, *65*, 103974. [[CrossRef](#)]
26. Gu, D.; Li, X.; Zhao, Y.; Wang, J. Enhanced NO₂ sensing of SnO₂/SnS₂ heterojunction based sensor. *Sens. Actuators B Chem.* **2017**, *244*, 67–76. [[CrossRef](#)]
27. Hao, J.; Zhang, D.; Sun, Q.; Zheng, S.; Sun, J.; Wang, Y. Hierarchical SnS₂/SnO₂ nanoheterojunctions with increased active-sites and charge transfer for ultrasensitive NO₂ detection. *Nanoscale* **2018**, *10*, 7210–7217. [[CrossRef](#)]
28. Wu, J.; Wu, Z.; Ding, H.; Wei, Y.; Huang, W.; Yang, X.; Li, Z.; Qiu, L.; Wang, X. Flexible, 3D SnS₂/Reduced graphene oxide heterostructured NO₂ sensor. *Sens. Actuators B Chem.* **2020**, *305*, 127445. [[CrossRef](#)]
29. Yu, J.; Xu, C.Y.; Ma, F.X.; Hu, S.P.; Zhang, Y.W.; Zhen, L. Monodisperse SnS₂ nanosheets for high-performance photocatalytic hydrogen generation. *ACS Appl. Mater. Interfaces* **2014**, *6*, 22370–22377. [[CrossRef](#)]
30. Zhang, D.; Zong, X.; Wu, Z.; Zhang, Y. Hierarchical Self-Assembled SnS₂ Nanoflower/Zn₂SnO₄ Hollow Sphere Nanohybrid for Humidity-Sensing Applications. *ACS Appl. Mater. Interfaces* **2018**, *10*, 32631–32639. [[CrossRef](#)]
31. Feng, Z.; Ma, Y.; Natarajan, V.; Zhao, Q.; Ma, X.; Zhan, J. In-situ generation of highly dispersed Au nanoparticles on porous ZnO nanoplates via ion exchange from hydrozincite for VOCs gas sensing. *Sens. Actuators B Chem.* **2018**, *255*, 884–890. [[CrossRef](#)]
32. Li, G.; Cheng, Z.; Xiang, Q.; Yan, L.; Wang, X.; Xu, J. Bimetal PdAu decorated SnO₂ nanosheets based gas sensor with temperature-dependent dual selectivity for detecting formaldehyde and acetone. *Sens. Actuators B Chem.* **2019**, *283*, 590–601. [[CrossRef](#)]
33. Suchomel, P.; Kvittek, L.; Pucek, R.; Panacek, A.; Halder, A.; Vajda, S.; Zboril, R. Simple size-controlled synthesis of Au nanoparticles and their size-dependent catalytic activity. *Sci. Rep.* **2018**, *8*, 4589. [[CrossRef](#)] [[PubMed](#)]
34. Najafshirtari, S.; Guardia, P.; Scarpellini, A.; Prato, M.; Marras, S.; Manna, L.; Colombo, M. The effect of Au domain size on the CO oxidation catalytic activity of colloidal Au-FeO_x dumbbell-like heterodimers. *J. Catal.* **2016**, *338*, 115–123. [[CrossRef](#)]
35. Wu, J.; Feng, S.; Li, Z.; Tao, K.; Chu, J.; Miao, J.; Norford, L.K. Boosted sensitivity of graphene gas sensor via nanoporous thin film structures. *Sens. Actuators B Chem.* **2018**, *255*, 1805–1813. [[CrossRef](#)]
36. Li, J.; Lu, Y.; Ye, Q.; Cinke, M.; Han, J.; Meyyappan, M. Carbon nanotube sensors for gas and organic vapor detection. *Nano Lett.* **2003**, *3*, 929–933. [[CrossRef](#)]
37. Nakate, U.T.; Bulakhe, R.N.; Lokhande, C.D.; Kale, S.N. Au sensitized ZnO nanorods for enhanced liquefied petroleum gas sensing properties. *Appl. Surf. Sci.* **2016**, *371*, 224–230. [[CrossRef](#)]
38. Wang, X.; Wang, J. Effects of Pt and Au adsorption on the gas sensing performance of SnS₂ monolayers: A DFT study. *Mater. Sci. Semicond. Process.* **2021**, *121*, 105416. [[CrossRef](#)]
39. Wang, F.; Wong, R.J.; Ho, J.H.; Jiang, Y.; Amal, R. Sensitization of Pt/TiO₂ Using Plasmonic Au Nanoparticles for Hydrogen Evolution under Visible-Light Irradiation. *ACS Appl. Mater. Interfaces* **2017**, *9*, 30575–30582. [[CrossRef](#)]
40. Yang, X.; Fu, H.; Tian, Y.; Xie, Q.; Xiong, S.; Han, D.; Zhang, H.; An, X. Au decorated In₂O₃ hollow nanospheres: A novel sensing material toward amine. *Sens. Actuators B Chem.* **2019**, *296*, 126696. [[CrossRef](#)]
41. Li, F.; Li, C.; Zhu, L.; Guo, W.; Shen, L.; Wen, S.; Ruan, S. Enhanced toluene sensing performance of gold-functionalized WO₃·H₂O nanosheets. *Sens. Actuators B Chem.* **2016**, *223*, 761–767. [[CrossRef](#)]
42. Xu, Y.; Ma, T.; Zheng, L.; Sun, L.; Liu, X.; Zhao, Y.; Zhang, J. Rational design of Au/Co₃O₄-functionalized W₁₈O₄₉ hollow heterostructures with high sensitivity and ultralow limit for triethylamine detection. *Sens. Actuators B Chem.* **2019**, *284*, 202–212. [[CrossRef](#)]